

# RSC Advances



This is an *Accepted Manuscript*, which has been through the Royal Society of Chemistry peer review process and has been accepted for publication.

*Accepted Manuscripts* are published online shortly after acceptance, before technical editing, formatting and proof reading. Using this free service, authors can make their results available to the community, in citable form, before we publish the edited article. This *Accepted Manuscript* will be replaced by the edited, formatted and paginated article as soon as this is available.

You can find more information about *Accepted Manuscripts* in the [Information for Authors](#).

Please note that technical editing may introduce minor changes to the text and/or graphics, which may alter content. The journal's standard [Terms & Conditions](#) and the [Ethical guidelines](#) still apply. In no event shall the Royal Society of Chemistry be held responsible for any errors or omissions in this *Accepted Manuscript* or any consequences arising from the use of any information it contains.

**New layer-by-layer Nb<sub>2</sub>O<sub>5</sub>/TiO<sub>2</sub> film as an effective underlayer in  
dye-sensitised solar cells**

L. F. Paula<sup>1</sup>, R. C. Amaral<sup>2</sup>, N. Y. Murakami Iha<sup>2</sup>, R. M. Paniago<sup>3</sup>, A. E. H.  
Machado<sup>1</sup>, A. O. T. Patrocínio\*<sup>1</sup>

<sup>1</sup> Instituto de Química, Universidade Federal de Uberlândia, 38400-902  
Uberlândia, MG, Brazil

<sup>2</sup> Laboratory of Photochemistry and Energy Conversion, LFCE, Instituto de  
Química, Universidade de São Paulo, 05508-900, São Paulo, SP, Brazil

<sup>3</sup> Departamento de Física, Universidade Federal de Minas Gerais 31270-010  
Belo Horizonte, MG, Brazil

\* to whom the correspondence should be addressed:

[otaviopatrocinio@iqufu.ufu.br](mailto:otaviopatrocinio@iqufu.ufu.br)

**Abstract**

Highly efficient all-inorganic  $\text{TiO}_2/\text{Nb}_2\text{O}_5$  underlayers for dye-sensitised solar cell applications were produced by the layer-by-layer technique (LbL).  $\text{TiO}_2$  and  $\text{Nb}_2\text{O}_5$  nanoparticles were prepared by the sol-gel method under acidic and alkaline conditions, respectively. The LbL films exhibited a very compact and homogeneous surface, as shown in FESEM and AFM images, which ensured a physical barrier between the electrolyte and the FTO surface, decreasing the dark current at this interface. Moreover, the rough film surface improved the physical interaction between the mesoporous  $\text{TiO}_2$  layer and the conductive substrate. The Ti(IV)/Nb(V) molar ratio in the films was 1.6, as determined by XPS, and it is controlled by the pH employed during the deposition process. The relative concentration of nanoparticles in the film plays a major role in its electronic properties: a higher  $\text{TiO}_2$  concentration allows an efficient transport of photoinjected electrons. Additionally, the presence of  $\text{Nb}_2\text{O}_5$  nanoparticles imposes an electronic barrier for charge transfer from the FTO to the electrolyte, as shown by electrochemical impedance spectroscopy. Thus, all the DSC photoelectrochemical parameters increased, leading to an expressive improvement in the overall conversion efficiency.

## 1. Introduction

Dye sensitised solar cells (DSCs) are a promising technology for cost-effective and highly efficient solar-to-electricity energy conversion.<sup>1-3</sup> Continuous research on materials,<sup>4-8</sup> device architecture<sup>9, 10</sup> as well as on electron transfer dynamics<sup>11-13</sup> has led to a continuous improvement in the conversion efficiency up to 15%.<sup>14</sup> Additionally, solar panels up to 6000 cm<sup>2</sup> have been reported, establishing the basis for future large scale production and commercialisation.<sup>15</sup>

Efficient solar energy conversion in DSCs requires the control of charge recombination at different device interfaces.<sup>12, 16-19</sup> In both liquid and solid-based DSCs, charge recombination at the FTO/electrolyte interface is one of the major charge loss pathways, which can be avoided by the deposition of compact oxide layers. These so-called blocking layers physically prevent contact between the oxidised species of the electrolyte and the conductive substrate, slowing down the charge recombination. They have been prepared by different techniques such as spray pyrolysis, sputtering and dip coating, among others.<sup>20-25</sup>

In previous contributions, we have described the application of the layer-by-layer (LbL) technique to produce efficient TiO<sub>2</sub> blocking layers for DSCs. LbL is a non-energy consumptive and easily upscalable technique that allows the deposition of compact oxide films with fine thickness control.<sup>26-30</sup> The efficiency of LbL compact TiO<sub>2</sub> films as blocking layers in DSCs is intrinsically related to the thermal stability of the polyelectrolyte employed as anions in the deposition. A lower polyanion mass loss during thermal treatment leads to a less porous film and a more effective blocking layer. Thus, it is desirable to replace the organic polyanion with an oxide-based material to avoid morphological changes

during the thermal treatment. A suitable candidate for production of all inorganic blocking layer is Nb<sub>2</sub>O<sub>5</sub>. The controlled hydrolysis of Nb(V) species at high pHs tend to produce hexaniobate anions that can replace the polyanions in the LbL films and will further produce Nb<sub>2</sub>O<sub>5</sub>·*n*H<sub>2</sub>O<sup>31</sup>. Additionally, Nb<sub>2</sub>O<sub>5</sub> does not absorb visible light and is a more insulate material than TiO<sub>2</sub>, which is an advantage for the blocking layer<sup>32</sup>.

In this work, we report an all-inorganic TiO<sub>2</sub>/Nb<sub>2</sub>O<sub>5</sub> film produced by the layer-by-layer technique that exhibits suitable morphological and electronic properties to be applied as underlayer in DSCs. The LbL TiO<sub>2</sub>/Nb<sub>2</sub>O<sub>5</sub> films were investigated by using different surface characterisation as well as electrochemical techniques, and successfully applied as underlayers in DSCs.

## 2. Experimental

All chemicals were analytical or HPLC grade and were used as received. The N3 dye, *cis*-[Ru(dcbH<sub>2</sub>)<sub>2</sub>(NCS)<sub>2</sub>], dcbH<sub>2</sub> = 4,4'-dicarboxylic acid-2,2'-bipyridine, was synthesised as previously reported<sup>33</sup> and used as a standard sensitiser.

The synthesis of TiO<sub>2</sub> or Nb<sub>2</sub>O<sub>5</sub> nanoparticles was performed by the sol-gel method under acidic and alkaline conditions, respectively. Positively charged TiO<sub>2</sub> nanoparticles were prepared by hydrolysis of titanium(IV) isopropoxide (Aldrich, 97%) in a 1 mol L<sup>-1</sup> HNO<sub>3</sub> aqueous solution, as previously reported.<sup>34</sup> Negatively charged Nb<sub>2</sub>O<sub>5</sub> nanoparticles were produced through the alkaline hydrolysis of niobium(V) ethoxide (Aldrich, 99%) using a variation of the method proposed by Özer et al.<sup>35</sup> Under an argon atmosphere, 2 mL of niobium(V) ethoxide (8 mmol) was slowly added to 40 mL of absolute ethanol, containing

60  $\mu\text{L}$  (1  $\mu\text{mol}$ ) of acetic acid, cooled in an ice bath and. The mixture was stirred for 2 h to yield a pale yellow solution, which was slowly added to 80 mL of pH = 10  $\text{NH}_4\text{OH}/\text{NH}_4\text{Cl}$  buffer. The mixture was left under stirring at  $80^\circ\text{C}$  for 8 h to yield a stable and translucent white sol.

$\text{TiO}_2/\text{Nb}_2\text{O}_5$  LbL films were deposited onto cleaned FTO substrates (Pilkington, TEC-15,  $15 \Omega/\square$  per square) as describe elsewhere.<sup>36</sup> The pre-cleaned substrate was alternatively immersed for 3 minutes in a  $10 \text{ mg mL}^{-1}$  suspension of positively charged  $\text{TiO}_2$  nanoparticles (pH = 2) and in a  $10 \text{ mg mL}^{-1}$   $\text{Nb}_2\text{O}_5$  sol at pH = 10.

The mesoporous  $\text{TiO}_2$  layer was deposited into bare or modified FTOs by serigraphy, using an 18NR-T  $\text{TiO}_2$  paste (Dye Sol). Two sequential depositions were performed in order to obtain c.a.  $10 \mu\text{m}$  thick films, which were sintered at  $500^\circ\text{C}$  for 30 minutes. N3 sensitisation was achieved by soaking the films in a saturated ethanolic solution. Solar cells were assembled in a sandwich-type arrangement using a sensitised  $\text{TiO}_2$  photoanode and a transparent Pt-covered FTO (Pilkington, TEC-15) as the counterelectrode. A solution of  $0.05 \text{ mol L}^{-1} \text{I}_2/0.5 \text{ mol L}^{-1} \text{LiI}/0.5 \text{ mol L}^{-1}$  pyridine in acetonitrile (Aldrich) and 3-methyl-2-oxazolidinone (90:10 v/v) was used as an electrolyte mediator<sup>37, 38</sup>.

The as-synthesised nanoparticles were characterised by X-ray diffraction analysis (XRD) using an XRD600 powder diffractometer (Shimadzu) operating at 40 kV and 30 mA employing  $\text{Cu K}\alpha$  radiation. The diffractograms were collected at  $0.02^\circ$  step in a  $20\text{-}90^\circ$  range. The film morphologies were evaluated by field-emission scanning electron microscopy (FESEM) using a JSM 7401F (JEOL) microscope, and by atomic force microscopy (AFM) using a SPM-9600 scanning probe microscope (Shimadzu). AFM images were registered under

contact mode at a scan rate of 1 Hz. Film thicknesses were measured with an P-16 Stylus (KLA Tencor) profilometer. X-ray photoelectron spectroscopy experiments were carried out using an ESCALAB 220ixL spectrometer (VG Scientific) equipped with a hemispherical electron energy analyser using Mg-K $\alpha$  radiation ( $h\nu = 1487$  eV), as previously reported.<sup>34</sup> The binding energies were measured with reference to the C 1s peak at 284.6 eV.

DSC photoelectrochemical parameters were determined from current-voltage curves obtained under simulated  $1000 \text{ W m}^{-2}$  AM 1.5D solar radiation (Newport/Oriel 91160) and registered with a PAR 273A galvanostat/potentiostat (EG&G Instruments) system, as previously reported.<sup>37, 39</sup> All photoelectrochemical parameters are the average values measured in, at least, three reproducible individual cells of each type of photoanode.

Electrochemical impedance spectra (EIS) of bare and modified FTOs were registered with a VersaSTAT 4 potentiostat (PAR-AMETEK) equipped with an impedance analyser. The measurements were performed in the absence of the mesoporous TiO<sub>2</sub> layer and the sensitizer in order to clearly identify the effect of the TiO<sub>2</sub>/Nb<sub>2</sub>O<sub>5</sub> bilayer on the electrochemical behaviour of the electrode. The measurements were carried out in two-electrode mode over a frequency range of  $10^6$ - $10^{-2}$  Hz under a 10 mV AC amplitude signal and using the same electrolyte and counterelectrode employed in the DSC characterisation. Data fits were performed using Z-view software (Scribner Associates).

### 3. Results and Discussion

The slow addition of Ti(IV) or Nb(V) alkoxides to, respectively, acidic and alkaline aqueous solutions under vigorous stirring resulted in production of very small nanoparticles, which remained stable as aqueous suspensions for 3-5 days at room temperature. As reported previously,<sup>40, 41</sup> the acidic hydrolysis of Ti(IV) isopropoxide yields 5-10 nm TiO<sub>2</sub> nanoparticles which exhibit relatively broad X-ray diffraction peaks characteristic of anatase nanocrystals.

For the synthesis of Nb<sub>2</sub>O<sub>5</sub> nanoparticles, the molecular precursor was diluted in ethanol containing a small amount of acetic acid, which strongly interacts with Nb<sup>+5</sup> centres, decreasing reactivity towards the gelation process. The slow addition of the diluted Nb(V) ethoxide ethanolic solution to pH 10 aqueous buffer led to the production of hexaniobate anionic species such as Nb<sub>6</sub>O<sub>19</sub><sup>8-</sup> that after continuous stirring and heating yielded Nb<sub>2</sub>O<sub>5</sub>•nH<sub>2</sub>O nanoparticles.<sup>31</sup> XRD analysis of the dried sol showed very broad halos, characteristic of an amorphous material.

Alternate immersion of FTO substrates into TiO<sub>2</sub> and Nb<sub>2</sub>O<sub>5</sub> sols resulted in the formation of layer-by-layer films. The FTO optical transmittance decreased almost linearly as the number of bilayers increased (Figure 1), indicating homogeneous growth of the film. After the deposition of 30 bilayers, the thickness of the film, determined by profilometry, was 900 ± 70 nm. A decrease in transmittance was also observed for TiO<sub>2</sub> LbL films employing polyanions instead of negatively charged Nb<sub>2</sub>O<sub>5</sub> nanoparticles<sup>36</sup>, which can be attributed to light scattering by oxide particles. Therefore, it is critical to control the size of both TiO<sub>2</sub> and Nb<sub>2</sub>O<sub>5</sub> nanoparticles and their agglomeration in order to avoid a

large decrease in substrate transmittance, which should cause losses in the DSC light harvesting efficiency.

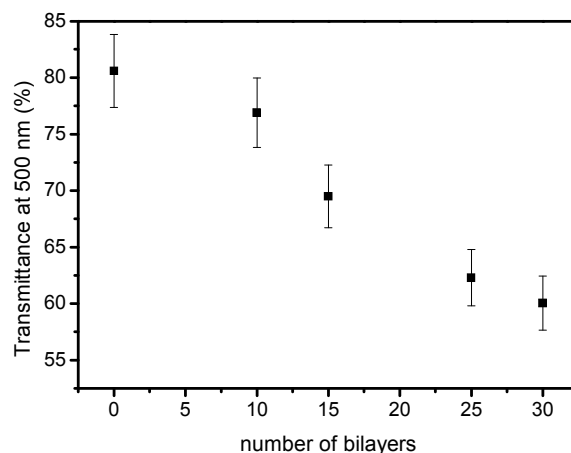


Figure 1. Transmittance changes in FTO as a function of the number of deposited  $\text{TiO}_2/\text{Nb}_2\text{O}_5$  bilayers.

The  $\text{TiO}_2/\text{Nb}_2\text{O}_5$  LbL films were sintered at  $450^\circ\text{C}$  after being dried at room temperature in order to ensure mechanical stability. The XRD pattern of the film, after thermal treatment, exhibited peaks ascribed mainly to the anatase  $\text{TiO}_2$  polymorph (Figure 2), which indicates that  $\text{Nb}_2\text{O}_5$  nanoparticles remained amorphous. The relative small intensity peak at  $2\theta \cong 30^\circ$  indicate the presence of a small amount of  $\text{TiO}_2$  in brookite phase. This result agrees with previous diffraction data obtained by Da Costa et al. for  $\text{Nb}_2\text{O}_5\text{-TiO}_2$  thin films prepared by the sol-gel sonocatalytic method and sintered at temperatures lower than  $500^\circ\text{C}$ .<sup>42</sup> Thus, it can be concluded that no crystalline new phases were formed after the thermal treatment and that only electrostatic interactions occurred between the  $\text{TiO}_2$  and  $\text{Nb}_2\text{O}_5$  nanoparticles.

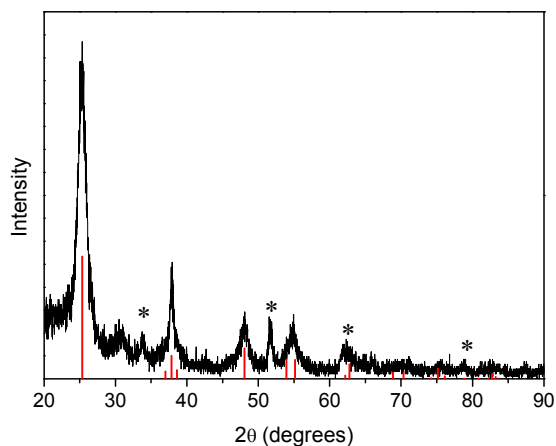


Figure 2. X-ray diffractogram of 30  $\text{TiO}_2/\text{Nb}_2\text{O}_5$  bilayers on the FTO surface. (\* indicates peaks from FTO. The vertical lines refer to the anatase diffraction peaks – JCPDS 21-1272).

X- ray phototelectron spectroscopy (XPS) confirmed the presence of Ti(IV) and Nb(V) ions on the FTO surface (Figure 3). The Ti(IV)/Nb(V) molar ratio was c.a. 1.6, which indicates the presence of more  $\text{TiO}_2$  nanoparticles than  $\text{Nb}_2\text{O}_5$  nanoparticles.

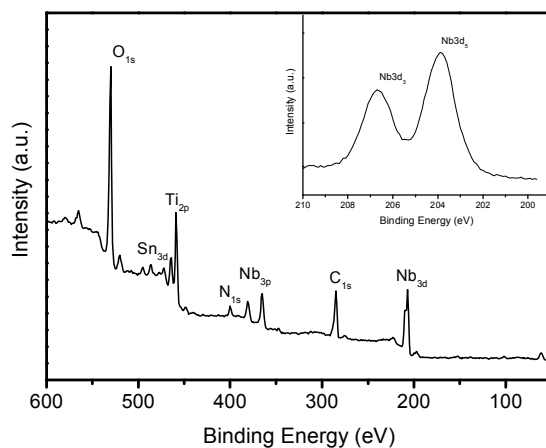


Figure 3. XPS survey spectrum of 30  $\text{TiO}_2/\text{Nb}_2\text{O}_5$  bilayers film on FTO. *Inset:* high resolution scan of Nb-3d peaks.

The relative concentrations of titanium(IV) and niobium(V) oxides are dependent on the superficial charges of each nanoparticle, which are determined by the pH of the sols employed in the LbL deposition. The higher concentration of TiO<sub>2</sub> nanoparticle indicates that its superficial charge at pH 2 was lower than that of Nb<sub>2</sub>O<sub>5</sub> at pH 10, and that more particles were necessary to reach the charge equilibrium at each deposition cycle. This result agrees with the expected production of highly charged anionic hexaniobate species during the controlled hydrolysis of Nb(V) ethoxide. Therefore, the Ti/Nb molar ratio can be controlled by the pH employed during the deposition process, but pH variations are limited by the stability of the sol. As the pH approaches the isoelectric point of the oxides (around 6 for TiO<sub>2</sub> and 4 for Nb<sub>2</sub>O<sub>5</sub><sup>43</sup>), the particles tend to aggregate and precipitate.

The morphology of the TiO<sub>2</sub>/Nb<sub>2</sub>O<sub>5</sub> films was evaluated by FEG-SEM and by AFM (Figure 4). One can observe a very homogeneous and compact film (Figure 4a) comprised of spherical particles with diameters less than 15 nm. The AFM images (Figure 4b) exhibit an irregular surface with RMS roughness of 65 ± 10 nm, calculated by the microscope software. In comparison to the previously reported LbL film prepared with acidic TiO<sub>2</sub> nanoparticles as cations and sulphonate polystyrene (PSS) as polyanions,<sup>36, 44</sup> the all-inorganic TiO<sub>2</sub>/Nb<sub>2</sub>O<sub>5</sub> films exhibited a more homogeneous morphology, without the characteristic plates that were observed for polyanion-based LbL films. Additionally, there was no mass loss during the sintering step, and the TiO<sub>2</sub>/Nb<sub>2</sub>O<sub>5</sub> film was less porous than the TiO<sub>2</sub>/PSS film.

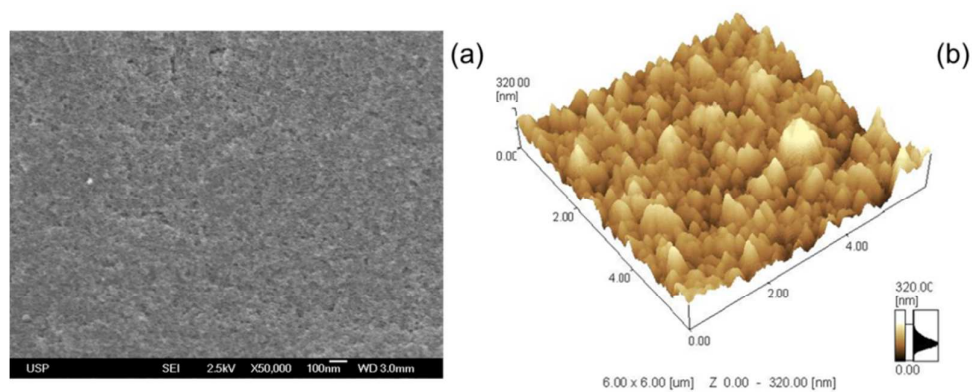


Figure 4. SEM (a) and AFM (b) images of 30 TiO<sub>2</sub>/Nb<sub>2</sub>O<sub>5</sub> bilayers deposited on the FTO.

Application of the TiO<sub>2</sub>/Nb<sub>2</sub>O<sub>5</sub> film as an underlayer in the photoanodes of DSCs resulted in an enhancement of all photoelectrochemical parameters (Table 1, Figure 5). The results show the effectiveness of these films as blocking/contact underlayer in DSCs. The relative increase in the DSC conversion efficiency due to the application of TiO<sub>2</sub>/Nb<sub>2</sub>O<sub>5</sub> films was higher than that previously observed for TiO<sub>2</sub> LbL films using polyanions<sup>36, 44, 45</sup> and also for blocking layers deposited by other techniques.<sup>21, 46, 47</sup>

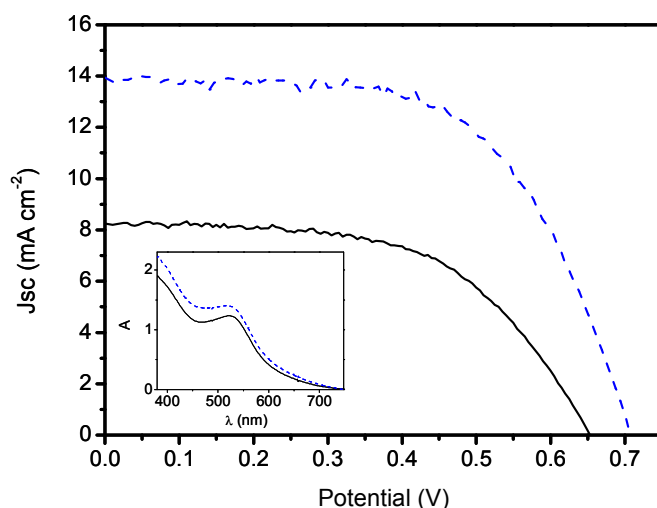


Figure 5. Current-voltage curves under A.M. 1.5 illumination ( $94.0 \text{ mW cm}^{-2}$ ) of DSCs without the blocking layer (—) or with 30  $\text{TiO}_2/\text{Nb}_2\text{O}_5$  bilayers (---). *Inset*: Electronic absorption spectra of the respective photoanodes sensitized by N3 (absorption from bare photoanodes have been subtracted).

Table 1. Photoelectrochemical parameters of DSCs with and without the  $\text{TiO}_2/\text{Nb}_2\text{O}_5$  underlayer (30 bilayers); AM 1.5 radiation;  $94 \text{ mW cm}^{-2}$ .

Photoanode	$j_{sc} (\text{mW cm}^{-2})$	$V_{oc} (\text{V})$	FF	$\eta (\%)$
Meso $\text{TiO}_2$	$8.3 \pm 0.5$	$0.67 \pm 0.01$	$0.57 \pm 0.01$	$3.3 \pm 0.2$
$\text{TiO}_2/\text{Nb}_2\text{O}_5$ -Meso $\text{TiO}_2$	$13.9 \pm 0.2$	$0.70 \pm 0.01$	$0.60 \pm 0.01$	$6.2 \pm 0.1$

The blocking effect due to the presence of the LbL  $\text{TiO}_2/\text{Nb}_2\text{O}_5$  underlayer was confirmed by the increase in the open-circuit voltage ( $V_{oc}$ ) in relation to DSCs employing bare FTOs and also by the decrease in the DSC dark current (Figure 6). The so-called dark current corresponds to triiodide reduction at the photoanode surface at a given potential. It can be observed that higher potentials were required to observe charge transfer from the photoanode to the  $\text{I}_3^-$  species in DSCs with the  $\text{TiO}_2/\text{Nb}_2\text{O}_5$  underlayer.

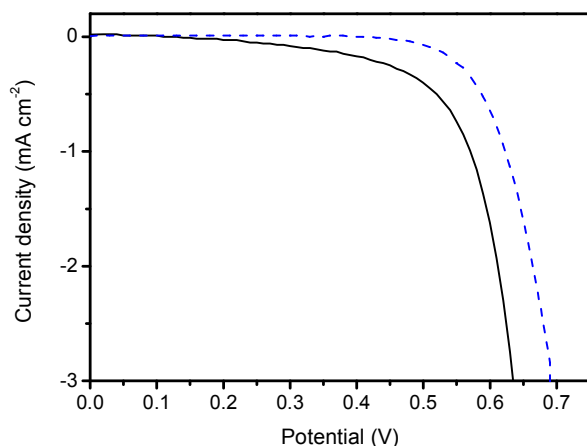


Figure 6. Dark current-voltage curves for DSCs without (—) and with (---) the  $\text{TiO}_2/\text{Nb}_2\text{O}_5$  film (30 bilayers).

It is also noteworthy to observe the enhancement in the short-circuit current due to the application of the LbL  $\text{TiO}_2/\text{Nb}_2\text{O}_5$  underlayer. The Incident light-to-current conversion efficiency (IPCE) spectrum of a DSC with the  $\text{TiO}_2/\text{Nb}_2\text{O}_5$  bilayer confirms the improvement in the photocurrent in relation to the a solar cell without the underlayer, Figure 7.

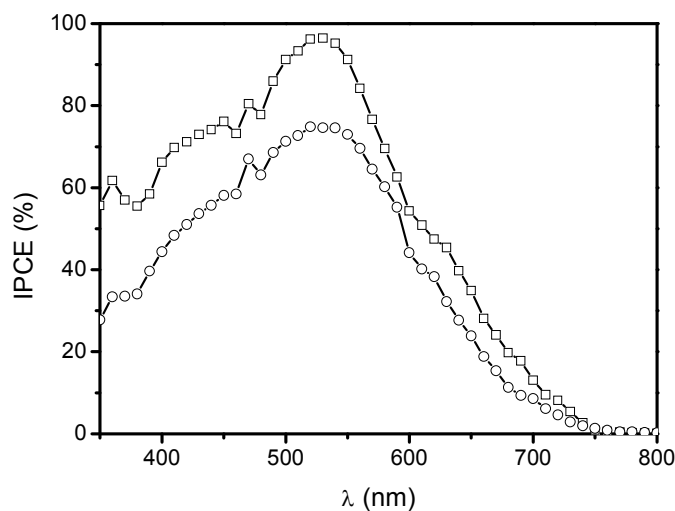


Figure 7. IPCE spectra of DSCs with ( $\square$ ) and without ( $\circ$ ) the  $\text{TiO}_2/\text{Nb}_2\text{O}_5$  bilayer.

This improvement can be partially explained by the c.a. 14% increase in the dye adsorption (Figure 5 inset). However, the light harvesting improvement due to the higher N3 concentration at the photoanode surface cannot be the only reason for the higher  $J_{sc}$  observed, since the presence of  $TiO_2/Nb_2O_5$  also decreased the FTO optical transmittance (see Figure 1). Thus, the LbL compact  $TiO_2/Nb_2O_5$  layer prevented electron recombination under open-circuit conditions as well as enhanced the electron collection efficiency on load and under short-circuit conditions. This behaviour was also observed by Lee et al. for Nb-doped  $TiO_2$  compact layers produced by pulsed layer deposition<sup>48</sup> and for other compact underlayers, such as those produced by  $TiCl_4$  treatment.<sup>47</sup> The beneficial improvement in the photocurrent due to the application of an LbL  $TiO_2/Nb_2O_5$  film can be related to its greater roughness in relation to the unmodified FTO surface. The rougher surface increases the interaction with the  $TiO_2$  mesoporous layer promoted by the sintering step and, consequently, enhances the electron collection efficiency at the FTO/ $TiO_2$  interface.

Electrochemical impedance spectroscopy (EIS) was employed to achieve a better understanding of the role of the  $TiO_2/Nb_2O_5$  compact film in the electron transfer processes. Bare or modified FTOs were set as working electrodes and a platinised FTO was used as the counter-electrode. As the electrolyte, the same composition was used as that employed in the J-V curve measurements. Figure 8(a) shows the Nyquist plots for FTO electrodes modified with 30  $TiO_2/Nb_2O_5$  bilayers at different bias. As expected, the system exhibited a strong capacitive behaviour at low applied potentials and became more conductive as the bias was increased. At -0.7 V, three distinct processes can be observed: the small semi-circle at high frequency is attributed to charge transfer

at the counterelectrode ( $RC_{ce}$ ).<sup>49-52</sup> A more capacitive response in the middle frequency range is ascribed to the working electrode ( $RC_{we}$ ) and, finally, lower frequency signals refer to Nernstian diffusion in the electrolyte ( $W_d$ ).<sup>50</sup> The unmodified FTO spectra (Figure 8(b)) exhibit similar features with an overlap of the working and counterelectrode responses. Thus, the presence of the  $TiO_2/Nb_2O_5$  bilayer shifted the working electrode signals to lower frequencies, as can clearly be seen in the Bode plot (Figure 9).

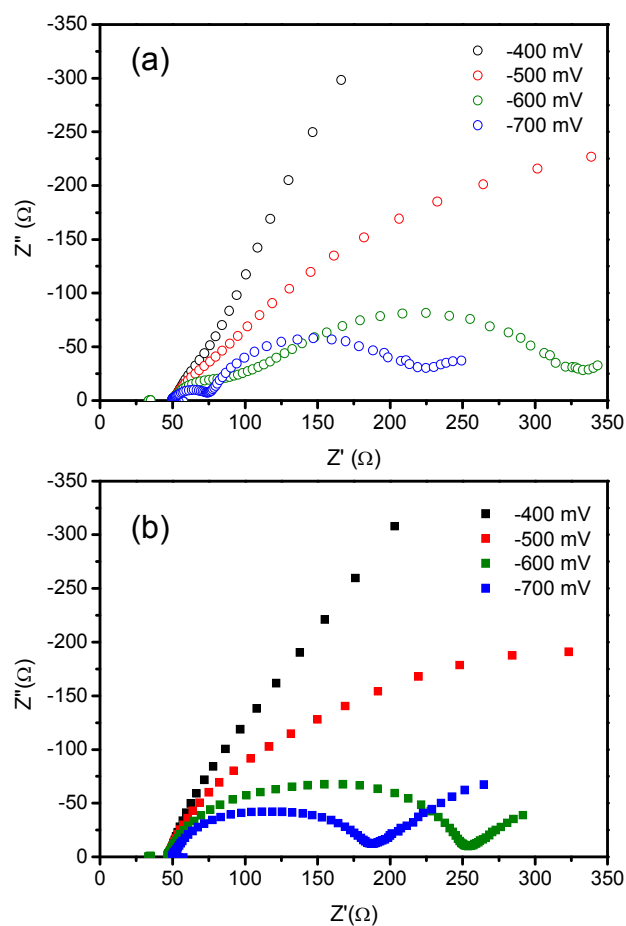


Figure 8. Nyquist plots of FTO electrodes with (a) and without (b) 30  $TiO_2/Nb_2O_5$  bilayers at different applied bias.

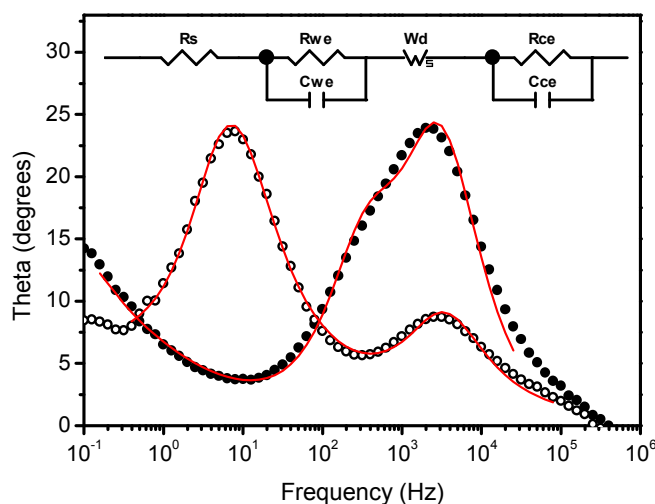


Figure 9. EIS spectra (Bode plots) of FTO electrodes with (○) and without (●) 30  $\text{TiO}_2/\text{Nb}_2\text{O}_5$  bilayers at -700 mV applied bias. The lines are the fits for the circuit shown as inset.

EIS data were fitted to the equivalent circuit shown as an inset in Figure 8. In the circuit,  $R_s$  is related to the working electrode sheet resistance that remained nearly the same for the bare and modified FTO. The shift of the working electrode phase angle peak to lower frequencies due to the presence of the  $\text{TiO}_2/\text{Nb}_2\text{O}_5$  underlayer indicated a lower current exchange rate for the modified FTO electrode. Based on the proposed equivalent circuit, the working electrode resistance ( $R_{we}$ ) and capacitance ( $C_{we}$ ) were determined as a function of applied bias, allowing us to estimate the associated electron exchange time constant ( $\tau_{we} = C_{we}R_{we}$ ) (Figure 10).

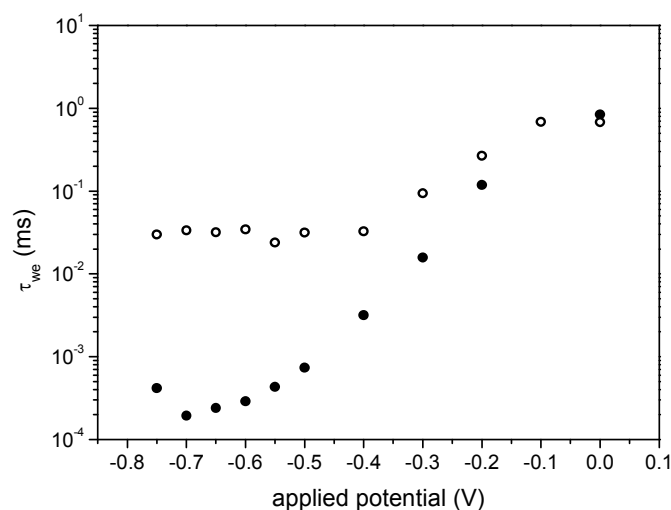


Figure 10. Semilogarithmic plots of the associated electron exchange lifetime ( $\tau_{we}$ ) as a function of the applied potential for the bare (●) and  $\text{TiO}_2/\text{Nb}_2\text{O}_5$  modified (○) FTO electrodes (30 bilayers).

In the unmodified FTO electrode, the electron exchange lifetime decreased as the applied potential became more negative, which means that electron transfer from the electrode to the electrolyte was faster. In the presence of the  $\text{TiO}_2/\text{Nb}_2\text{O}_5$  film,  $\tau_{we}$  exhibited an initial decrease as the potential changed from 0 to -0.4 V, and remained almost constant at more negative potentials. This behaviour is consistent with the expected blocking effect due to deposition of the compact  $\text{TiO}_2/\text{Nb}_2\text{O}_5$  layer.

The all-inorganic  $\text{TiO}_2/\text{Nb}_2\text{O}_5$  blocking layer exhibited better electrochemical behaviour than the  $\text{TiO}_2/\text{PSS}$  layer previously reported.<sup>44</sup> The polyanionic-based layer also increased the electron exchange lifetime in comparison to the bare FTO, although the layer was sufficiently conductive and  $\tau_{we}$  decayed exponentially at potentials more negative than -0.5 V. The better performance of the  $\text{TiO}_2/\text{Nb}_2\text{O}_5$  bilayer as a blocking/compact layer may be associated to the electronic properties of niobium(V) oxide. The conduction

band potential of  $\text{Nb}_2\text{O}_5$  is c.a. 0.1-0.3 V more negative than that observed for anatase  $\text{TiO}_2$ <sup>53-55</sup>. Thus, in the  $\text{TiO}_2/\text{Nb}_2\text{O}_5$  compact film, the energy barrier for the electron transfer from the FTO to the electrolyte should be c.a. 200-400 meV higher than in pure  $\text{TiO}_2$  films. The more capacitive behaviour observed for the  $\text{TiO}_2/\text{Nb}_2\text{O}_5$  modified FTOs in electrochemical impedance spectroscopy is in agreement with such a prediction. Therefore,  $\text{TiO}_2/\text{Nb}_2\text{O}_5$  blocking layers not only physically prevented contact between the electrolyte and the FTO surface, but also caused an electronic blocking for the charge recombination process at the FTO/electrolyte interface.

The electronic blocking effect was also observed by Xia and co-workers for pure  $\text{Nb}_2\text{O}_5$  thin layers deposited by radio frequency magnetron sputtering.<sup>32, 56</sup> Interestingly, the authors observed that only the application of very thin (<10 nm)  $\text{Nb}_2\text{O}_5$  layers resulted in an improvement in the DSC conversion efficiency. If thicker films were employed, the conversion efficiencies decreased significantly due to the reduction in electron transport efficiency caused by the highly capacitive  $\text{Nb}_2\text{O}_5$  layer. For LbL  $\text{TiO}_2/\text{Nb}_2\text{O}_5$  films, the high Ti(IV)/Nb(V) ratio ensured an efficient electron transport even in thicker films, as can be observed from the high photocurrent determined for the DSCs employing 900 nm thick LbL films. Further experiments on the influence of number of  $\text{TiO}_2/\text{Nb}_2\text{O}_5$  bilayers on the DSC efficiency and in the electrochemical properties of the electrodes are going to be helpful to better understand the role of thickness on the LbL films effectiveness. Nevertheless, by the layer-by-layer assembly of  $\text{TiO}_2$  and  $\text{Nb}_2\text{O}_5$  nanoparticles, it was possible to combine efficient physical blocking with an electronic barrier to produce highly efficient compact underlayers for dye-sensitised solar cells.

#### 4. Conclusions

All-inorganic  $\text{TiO}_2/\text{Nb}_2\text{O}_5$  thin films were prepared by the layer-by-layer technique and efficiently applied as a blocking/contact underlayer in dye-sensitised solar cells. The relative amount of  $\text{TiO}_2$  and  $\text{Nb}_2\text{O}_5$  in the films is dependent on the pH of the sols employed during deposition. Surface characterisation showed that the LbL  $\text{TiO}_2/\text{Nb}_2\text{O}_5$  exhibited a very homogeneous and compact surface, which provided a physical barrier to the contact between the oxidised species in the electrolyte and the FTO surface. Moreover, the application of  $\text{TiO}_2/\text{Nb}_2\text{O}_5$  bilayers increased the roughness of the electrode surface, allowing a better interaction with the mesoporous layer. The high Ti/Nb molar ratio ensured efficient electron transport even for thicker films. As a result, higher  $J_{sc}$  and  $V_{oc}$  were achieved and an 87% improvement in the overall conversion efficiency was observed.

Electrochemical impedance measurements showed that the  $\text{TiO}_2/\text{Nb}_2\text{O}_5$  bilayers also exhibited an electronic blocking effect for charge recombination at the FTO surface due to the more negative potential of the  $\text{Nb}_2\text{O}_5$  conduction band. The electron exchange rates at the FTO decreased by at least one order of magnitude due to the presence of  $\text{TiO}_2/\text{Nb}_2\text{O}_5$ , which is in agreement with the higher open-circuit voltages observed for the DSCs with this blocking layer. Thus, the all-inorganic  $\text{TiO}_2/\text{Nb}_2\text{O}_5$  compact films prepared by a relatively simple and non-energy consumptive technique are a viable option for the production of highly efficient dye-sensitised solar cells.

## 5. Acknowledgments

This work was supported by Fundação de Amparo à Pesquisa do Estado de Minas Gerais (FAPEMIG), Fundação de Amparo à Pesquisa do Estado de São Paulo (FAPESP), Conselho Nacional de Desenvolvimento Científico e Tecnológico (CNPq) and Coordenação de Aperfeiçoamento de Pessoal de Nível Superior (CAPES). The authors are also thankful to the Multi-User Laboratory of Universidade Federal de Uberlândia by the AFM and XRD analyses.

## 6. References

1. B. O'Regan and M. Grätzel, *Nature*, 1991, **353**, 737-740.
2. A. Yella, H.-W. Lee, H. N. Tsao, C. Yi, A. K. Chandiran, M. K. Nazeeruddin, E. W.-G. Diau, C.-Y. Yeh, S. M. Zakeeruddin and M. Grätzel, *Science*, 2011, **334**, 629-634.
3. L. M. Peter, *J. Phys. Chem. Let.*, 2011, **2**, 1861-1867.
4. P. M. Sommeling, B. C. O'Regan, R. R. Haswell, H. J. P. Smit, N. J. Bakker, J. J. T. Smits, J. M. Kroon and J. A. M. van Roosmalen, *J. Phys. Chem. B*, 2006, **110**, 19191-19197.
5. J. Cong, X. Yang, L. Kloo and L. Sun, *En. Envir. Sci.*, 2012, **5**, 9180-9194.
6. L.-L. Li and E. W.-G. Diau, *Chem. Soc. Rev.*, 2013, **42**, 291-304.
7. S. Yang, Y. Hou, B. Zhang, X. H. Yang, W. Q. Fang, H. J. Zhao and H. G. Yang, *J. Mat. Chem. A*, 2013, **1**, 1374-1379.
8. X. Yan, L. Feng, J. Jia, X. Zhou and Y. Lin, *J. Mat. Chem. A*, 2013, **1**, 5347-5352.
9. J. M. Kroon, N. J. Bakker, H. J. P. Smit, P. Liska, K. R. Thampi, P. Wang, S. M. Zakeeruddin, M. Grätzel, A. Hinsch, S. Hore, U. Wurfel, R. Sastrawan, J. R. Durrant, E. Palomares, H. Pettersson, T. Gruszecki, J. Walter, K. Skupien and G. E. Tullloch, *Prog. Photovolt.*, 2007, **15**, 1-18.
10. L. H. Hu, S. Y. Dai, J. Weng, S. F. Xiao, Y. F. Sui, Y. Huang, S. H. Chen, F. T. Kong, X. Pan, L. Y. Liang and K. J. Wang, *J. Phys. Chem. B*, 2007, **111**, 358-362.
11. B. O'Regan, X. Li and T. Ghaddar, *En. Envir. Sci.*, 2012, **5**, 7203-7215.
12. L. Peter, *Acc. Chem. Res.*, 2009, **42**, 1839-1847.
13. B. C. O'Regan and J. R. Durrant, *Acc. Chem. Res.*, 2009, **42**, 1799-1808.
14. J. Burschka, N. Pellet, S. J. Moon, R. Humphry-Baker, P. Gao, M. K. Nazeeruddin and M. Grätzel, *Nature*, 2013, **499**, 316.
15. A. Hinsch, W. Veurman, H. Brandt, R. Loayza Aguirre, K. Bialecka and K. Flarup Jensen, *Prog. Photovolt.*, 2012, **20**, 698-710.

16. S. Ruehle, S. Yahav, S. Greenwald and A. Zaban, *J. Phys. Chem. C*, 2012, **116**, 17473-17478.
17. H. K. Dunn and L. M. Peter, *J. Phys. Chem. C*, 2009, **113**, 4726-4731.
18. P. J. Cameron, L. M. Peter and S. Hore, *J. Phys. Chem. B*, 2005, **109**, 930-936.
19. P. J. Cameron and L. M. Peter, *J. Phys. Chem. B*, 2005, **109**, 7392-7398.
20. Y. Wang, C. Chen, X. Cui, Y. Gu, Y. Zhang and Y. Sun, *Nano Sci. Nano Technol.*, 2013, **5**, 293-296.
21. X. Li, Y. Qiu, S. Wang, S. Lu, R. I. Gruar, X. Zhang, J. A. Darr and T. He, *Phys. Chem. Chem. Phys.*, 2013, **15**, 14729-14735.
22. T.-Y. Cho, K.-W. Ko, S.-G. Yoon, S. S. Sekhon, M. G. Kang, Y.-S. Hong and C.-H. Han, *Curr. Appl. Phys.*, 2013, **13**, 1391-1396.
23. H. Seo, M.-K. Son, S. Park, H.-J. Kim and M. Shiratani, *J Photochem. Photobiol A: Chem.*, 2012, **248**, 50-54.
24. C. S. Kovash, Jr., J. D. Hoefelmeyer and B. A. Logue, *Electrochim. Acta*, 2012, **67**, 18-23.
25. M. Liberatore, L. Burtone, T. M. Brown, A. Reale, A. Di Carlo, F. Decker, S. Caramori and C. A. Bignozzi, *Appl. Phys. Lett.*, 2009, **94**.
26. P.-Y. Chen, R. Ladewski, R. Miller, X. Dang, J. Qi, F. Liau, A. M. Belcher and P. T. Hammond, *J. Mat. Chem. A*, 2013, **1**, 2217-2224.
27. S. Yuan, R. Mao, Y. Li, Q. Zhang and H. Wang, *Electrochim. Acta*, 2012, **60**, 347-353.
28. S. Guldin, P. Docampo, M. Stefik, G. Kamita, U. Wiesner, H. J. Snaith and U. Steiner, *Small*, 2012, **8**, 432-440.
29. S. Srivastava and N. A. Kotov, *Acc. Chem. Res.*, 2008, **41**, 1831-1841.
30. L. G. Paterno and M. A. G. Soler, *Jom-U.S.*, 2013, **65**, 709-719.
31. J.-M. Jehng and I. E. Wachs, *Catal. Today*, 1990, **8**, 37-55.
32. J. Xia, N. Masaki, K. Jiang and S. Yanagida, *Chem. Commun.*, 2007, 138-140.
33. M. K. Nazeeruddin, A. Kay, I. Rodicio, R. Humphrybaker, E. Muller, P. Liska, N. Vlachopoulos and M. Grätzel, *J. Am. Chem. Soc.*, 1993, **115**, 6382-6390.
34. A. O. T. Patrocínio, E. B. Paniago, R. M. Paniago and N. Y. Murakami Iha, *Appl. Surf. Sci.*, 2008, **254**, 1874-1879.
35. N. Ozer, D. G. Chen and C. M. Lampert, *Thin Solid Films*, 1996, **277**, 162-168.
36. A. O. T. Patrocínio, L. G. Paterno and N. Y. Murakami Iha, *J Photochem. Photobiol A: Chem.*, 2009, **205**, 23-27.
37. A. O. T. Patrocínio and N. Y. Murakami Iha, *Quim. Nova*, 2010, **33**, 574-578.
38. C. G. Garcia and N. Y. Murakami Iha, *Inter. J. Photoen.*, 2001, **3**, 131-151.
39. A. O. T. Patrocínio, A. S. El-Bacha, E. B. Paniago, R. M. Paniago and N. Y. Murakami Iha, *Inter. J. Photoen.*, 2012, **638571**, 1-7.
40. K. Kalyanasundaram and M. Grätzel, *Coord. Chem. Rev.*, 1998, **177**, 347-414.
41. C. J. Barbe, F. Arendse, P. Comte, M. Jirousek, F. Lenzmann, V. Shklover and M. Grätzel, *J. Am. Ceram. Soc.*, 1997, **80**, 3157-3171.
42. E. Da Costa, C. O. Avellaneda and A. Pawlicka, *J. Mater. Sci.*, 2001, **36**, 1407-1410.
43. M. Kosmulski, E. Maczka and J. B. Rosenholm, *J. Phys. Chem. B*, 2002, **106**, 2918-2921.

44. A. O. T. Patrocinio, L. G. Paterno and N. Y. Murakami Iha, *J. Phys. Chem. C*, 2010, **114**, 17954-17959.
45. S. Yuan, Y. Li, Q. Zhang and H. Wang, *Electrochim. Acta*, 2012, **79**, 182-188.
46. J. Kim and J. Kim, *J. Nanosci. Nanotechnol.*, 2011, **11**, 7335-7338.
47. S. Ito, P. Liska, P. Comte, R. L. Charvet, P. Pechy, U. Bach, L. Schmidt-Mende, S. M. Zakeeruddin, A. Kay, M. K. Nazeeruddin and M. Grätzel, *Chem. Commun.*, 2005, 4351-4353.
48. S. Lee, J. H. Noh, H. S. Han, D. K. Yim, D. H. Kim, J. K. Lee, J. Y. Kim, H. S. Jung and K. S. Hong, *J. Phys. Chem. C*, 2009, **113**, 6878-6882.
49. M. S. Góes, E. Joanni, E. C. Muniz, R. Savu, T. R. Habeck, P. R. Bueno and F. Fabregat-Santiago, *J. Phys. Chem. C*, 2012, **116**, 12415-12421.
50. F. Fabregat-Santiago, J. Bisquert, G. Garcia-Belmonte, G. Boschloo and A. Hagfeldt, *Sol. Energy Mater. Sol. Cells*, 2005, **87**, 117-131.
51. M. Wang, P. Chen, R. Humphry-Baker, S. M. Zakeeruddin and M. Grätzel, *ChemPhysChem*, 2009, **10**, 290-299.
52. J. F. Shi, J. Liang, S. J. Peng, W. Xu, J. Pei and J. Chen, *Solid State Sci.*, 2009, **11**, 433-438.
53. K. Sayama, H. Sugihara and H. Arakawa, *Chem. Mater.*, 1998, **10**, 3825-3832.
54. D. E. Scaife, *Solar Energy*, 1980, **25**, 41-54.
55. H. P. Maruska and A. K. Ghosh, *Solar Energy*, 1978, **20**, 443-458.
56. J. B. Xia, N. Masaki, K. J. Jiang and S. Yanagida, *J. Photochem. Photobiol. A:Chem.*, 2007, **188**, 120-127.